

Supporting Information

Planar Defect-Driven Electrocatalysis of CO₂-to-C₂H₄ Conversion

Zhengyuan Li,^a Yanbo Fang,^b Jianfang Zhang,^a Tianyu Zhang,^a Juan D. Jimenez,^c Sanjaya D. Senanayake,^c Vesselin Shanov,^{ab} Shize Yang,^{*d} and Jingjie Wu^{*a}

^a. Department of Chemical and Environmental Engineering, University of Cincinnati, Cincinnati, OH 45221, USA

^b. Department of Mechanical and Materials Engineering, University of Cincinnati, Cincinnati, OH 45221, USA

^c. Chemistry Division, Brookhaven National Laboratory, Upton, NY 11973, USA

^d. Eyring Materials Center, Arizona State University, Tempe, AZ 85287, USA

* Corresponding authors: E-mail: jingjie.wu@uc.edu and shize.yang@asu.edu

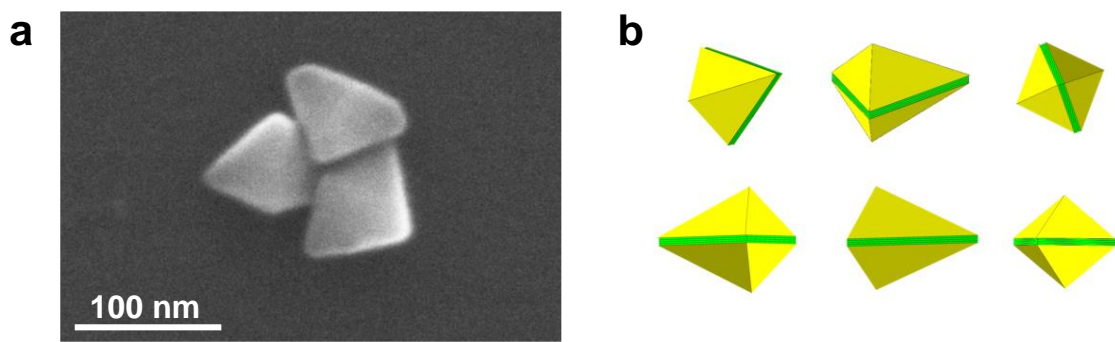


Fig. S1 (a) The high-magnification SEM image of the Rpb-Cu. (b) Schematic models of individual Rpb-Cu in different orientations. In each model, yellow and green represent (100) facets and planar defects, respectively.

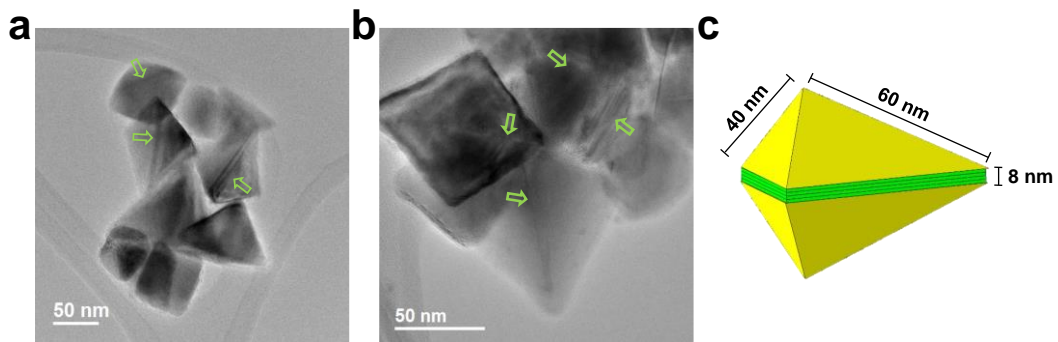


Fig. S2 (a, b) TEM images of the Rbp-Cu. The arrows denote the planar defects. (c) The dimensions of a typical Rbp-Cu NC were obtained from the TEM images. The proportion of the defects is calculated to be 20.1% from the geometric dimensions.

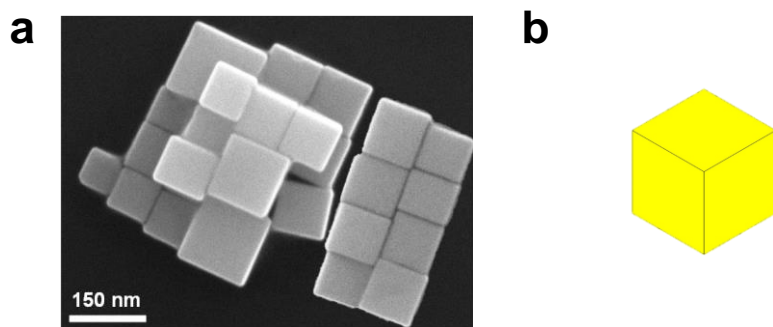


Fig. S3 (a) The high-magnification SEM image of the Cube-Cu. (b) Schematic mole of an individual Cube-Cu. Yellow represents (100) facets.

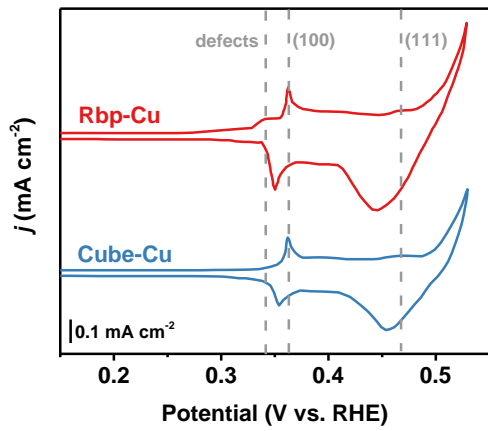


Fig. S4 CV curves for OH^- adsorption were performed in N_2 -saturated 0.1 M KOH at a scan rate of 20 mV s^{-1} . The peaks shown between $0.35 \sim 0.50 \text{ V}$ for Rbp-Cu and Cube-Cu can be assigned to (100) facets at *ca.* 0.36 V and (111) facets at *ca.* 0.46 V . An additional shoulder peak at *ca.* 0.34 V for Rbp-Cu is associated with surface defects.^{S1,S2}

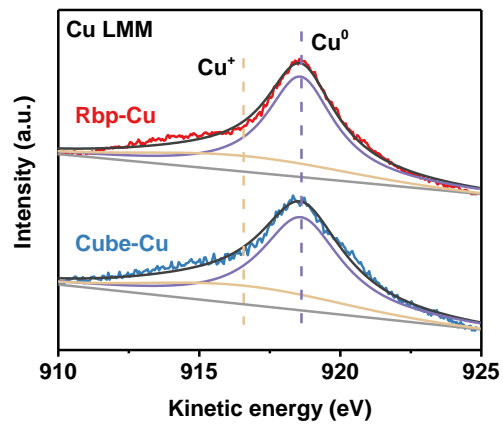


Fig. S5 Cu LMM spectrum for the Rbp-Cu and Cube-Cu.

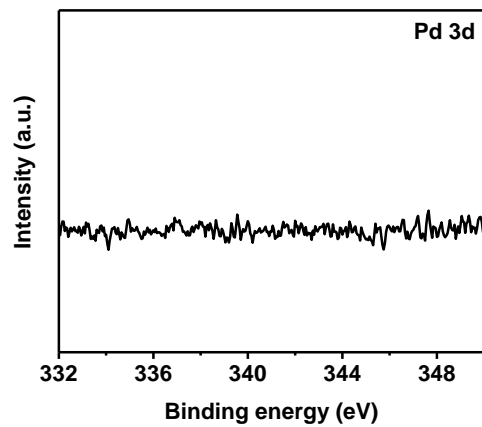


Fig. S6 Pd 3d XPS spectrum for the Rbp-Cu.

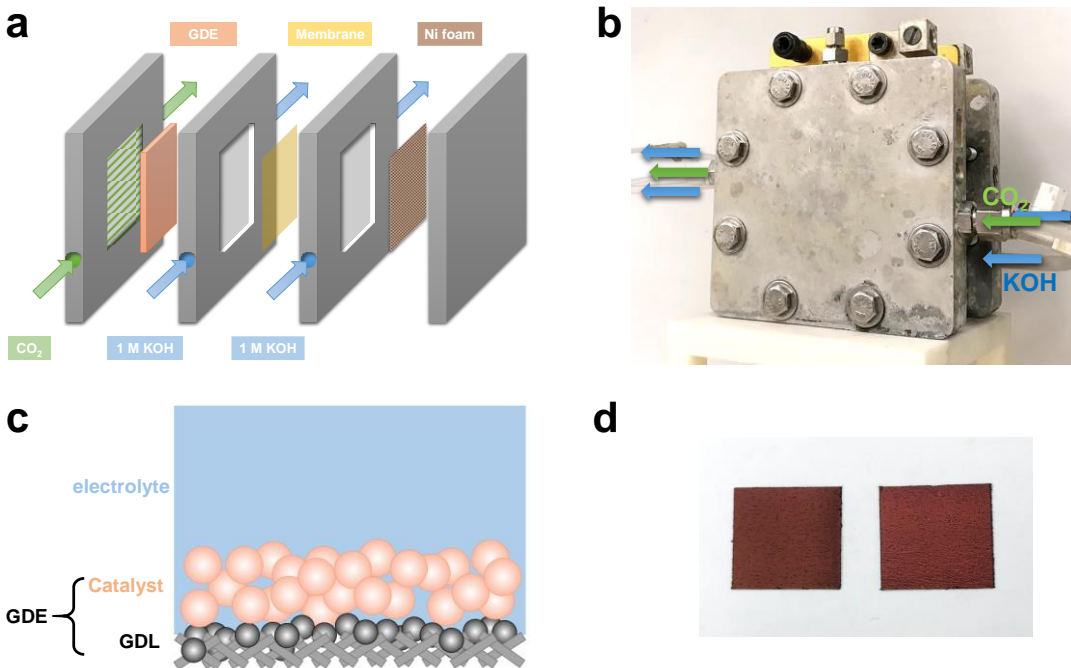


Fig. S7 (a) Schematic and (b) photo of a customized flow cell. (c) Schematic and (d) photo of GDE (left: Rbp-Cu; right: Cube-Cu).

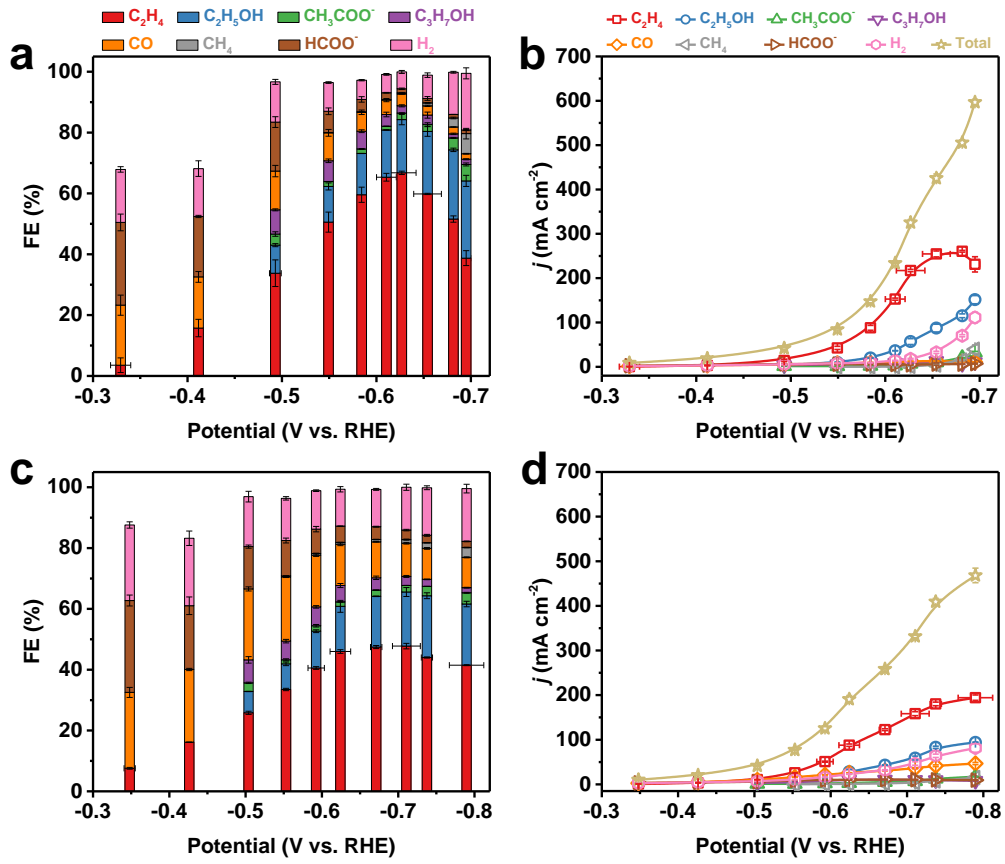


Fig. S8 CO₂RR performance for (a, b) Rbp-Cu, and (c, d) Cube-Cu in the flow cell with 1 M KOH. The error bars represent one standard deviation based on the measurements of three independent electrodes.

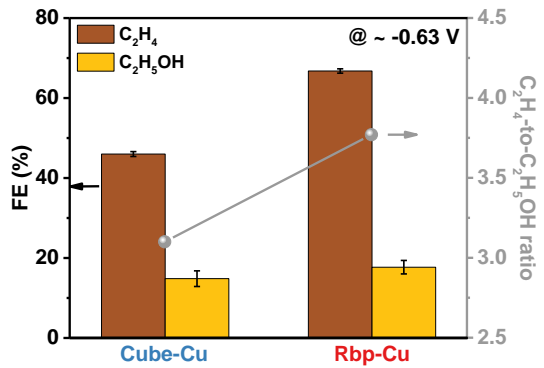


Fig. S9 The FE of C_2H_4 and $\text{C}_2\text{H}_5\text{OH}$, and their ratio for Rbp-Cu and Cube-Cu at -0.63 V vs. RHE.

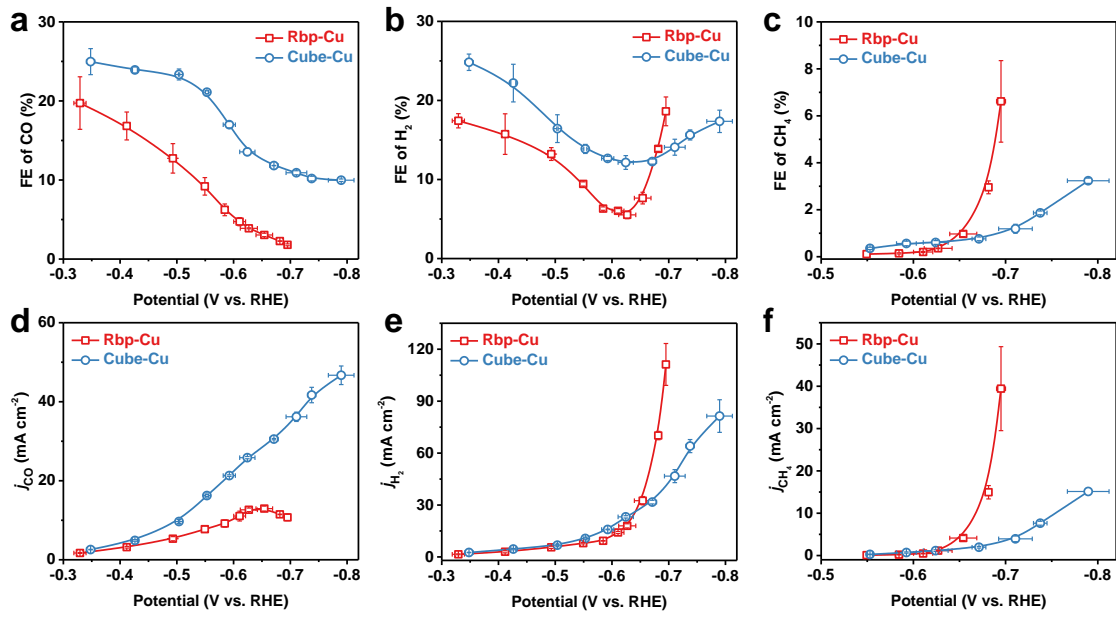


Fig. S10 Comparison of the FE of (a) CO, (b) H₂, and (c) CH₄ for the Rbp-Cu and Cube-Cu under different applied potentials. Comparison of the partial current density of (d) CO, (e) H₂, and (f) CH₄ for the Rbp-Cu and Cube-Cu under different applied potentials.

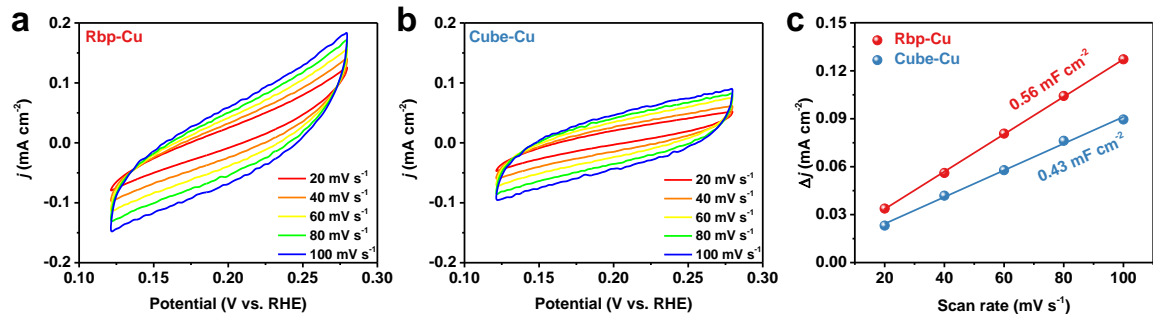


Fig. S11 CV curves of (a) Rbp-Cu and (b) Cube-Cu with various scan rates from 20 mV s^{-1} to 100 mV s^{-1} . (c) The determination of C_{dl} for each samples. The C_{dl} was estimated by plotting the $\Delta j = (j_a - j_c)$ at 0.20 V vs. RHE (where j_c and j_a are the cathodic and anodic current densities, respectively) against the scan rates. The fitting slope value is twice that of the C_{dl} .

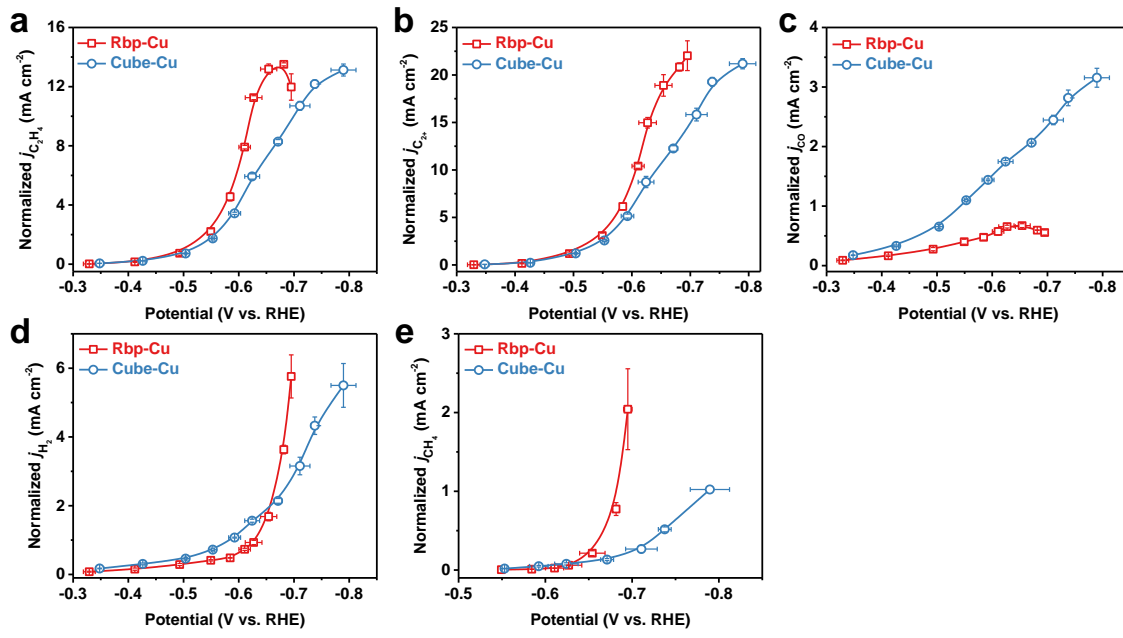


Fig. S12 Comparison of the ECSA normalized current density of (a) C_2H_4 , (b) C_2^+ products, (c) CO, (d) H_2 , and (e) CH_4 for the Rbp-Cu and Cube-Cu under different applied potentials. The ECSA normalized current density was corrected from geometric current density by a factor of $C_{\text{dl}}/C_{\text{cu}}$, where C_{cu} is the capacitance of polycrystalline Cu foil ($29 \mu\text{F cm}^{-2}$).^{S3}

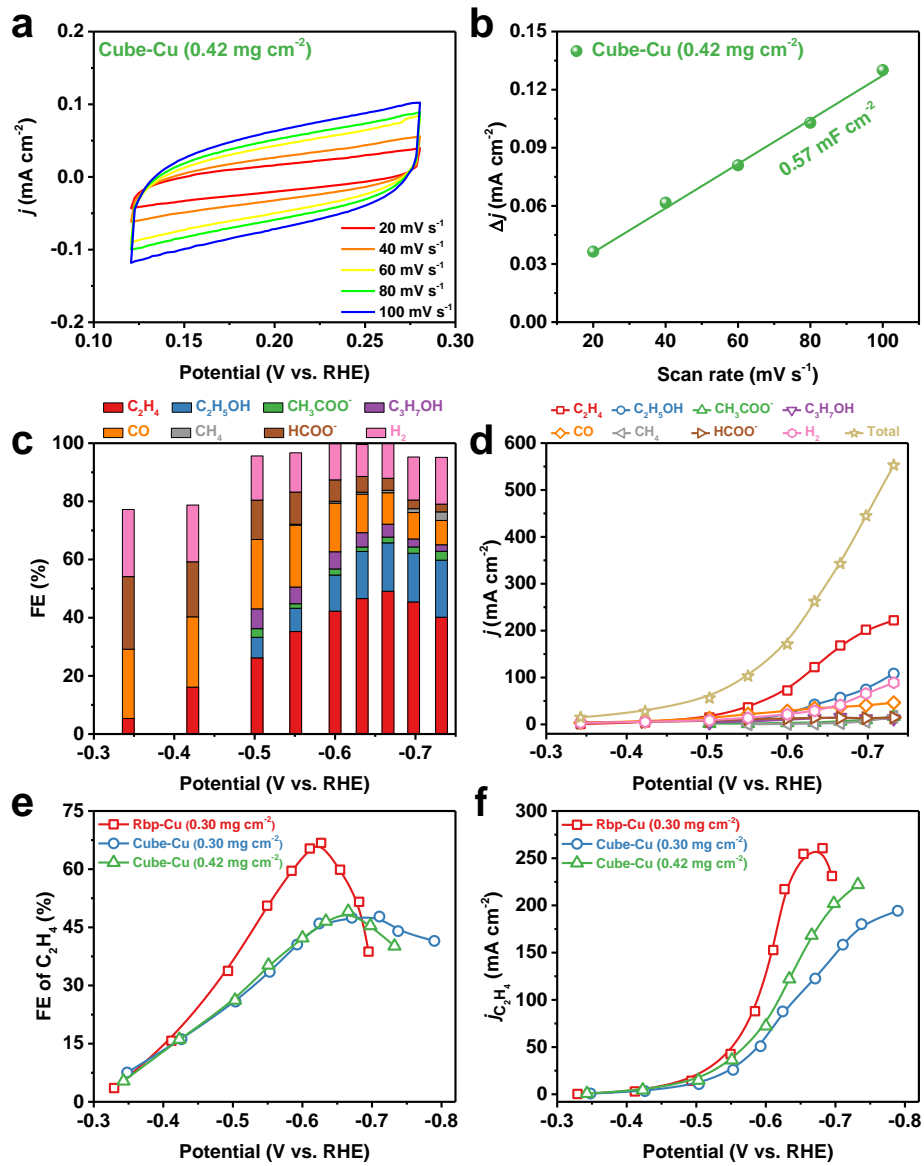


Fig. S13 (a) CV curves, (b) the determination of C_{dl} , and (c, d) CO₂RR performance for the Cube-Cu with a higher loading of 0.42 mg cm^{-2} . Comparison of (e) FE of C_2H_4 and (f) $j_{\text{C}_2\text{H}_4}$ for Rbp-Cu (0.30 mg cm^{-2}), Cube-Cu (0.30 mg cm^{-2}) and Cube-Cu (0.42 mg cm^{-2}).

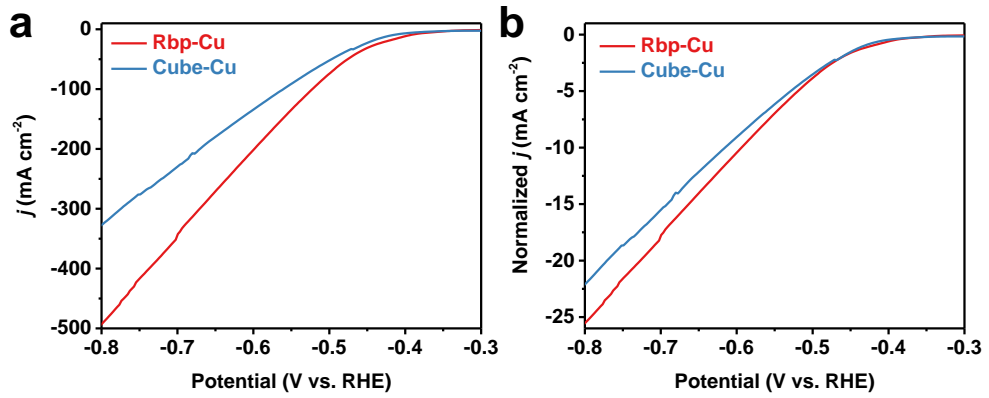


Fig. S14 (a) LSV curves and (b) ECSA normalized LSV curves for the Rbp-Cu and Cube-Cu measured in a flow cell with Ar and 1 M KOH.

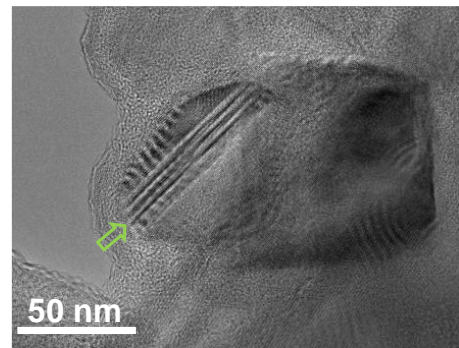


Fig. S15 TEM image of the Rbp-Cu after CO₂RR. The arrow denotes the planar defects.

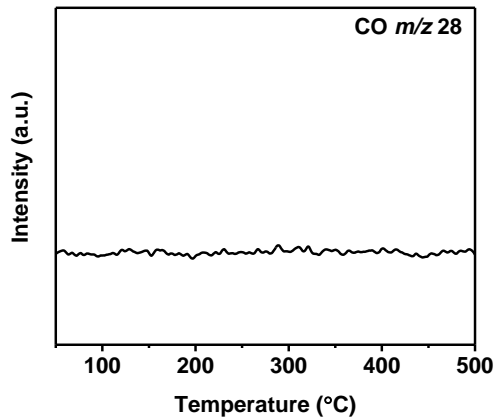


Fig. S16 CO-TPD profile of alumina support. The pure alumina cannot adsorb CO, excluding its adsorption effect.

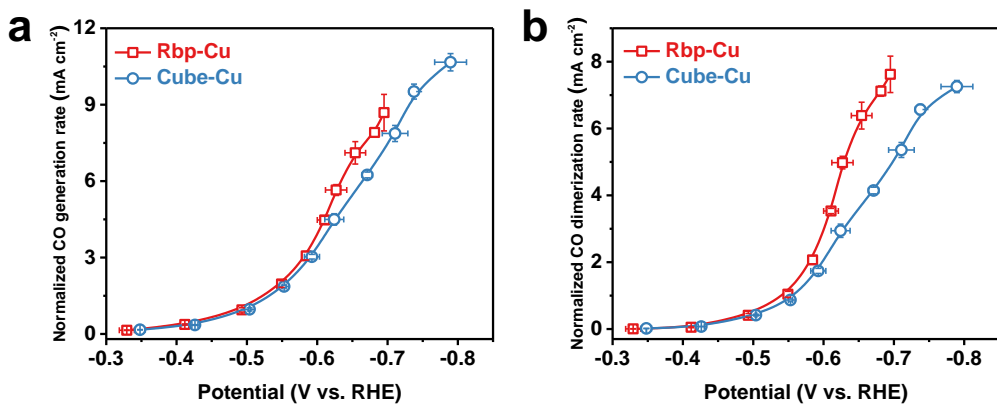


Fig. S17 Comparison of the ECSA normalized (a) CO generation rate and (b) CO dimerization rate for the Rbp-Cu and Cube-Cu under different applied potentials.

Table S1. Comparison of CO₂RR towards C₂H₄ of Rbp-Cu with those of state-of-the-art electrocatalysts using the flow cell with 1 M KOH

Catalyst	Potential (V vs. RHE)	FE of C ₂ H ₄ (%)	$j_{C_2H_4}$ (mA cm ⁻²)	Reference
Rbp-Cu	-0.63	67	217	This work
Cu(OH) ₂ -D	-0.54	58	146	S4
CuAg alloy	-0.68	60	170	S5
Nanoporous Cu	-0.67	39	258	S6
Cu-1	-0.79	46	140	S7
GB-Cu	-1.20	38	39	S8
CuDAT-wire	-0.60	40	65	S9
Cu nanocube	-0.80	51	82	S10
CuO/ZnO/C	-0.74	46	156	S11

References

- S1. D. Raciti, L. Cao, K. J. T. Livi, P. F. Rottmann, X. Tang, C. Li, Z. Hicks, K. H. Bowen, K. J. Hemker, T. Mueller and C. Wang, *ACS Catal.*, 2017, **7**, 4467–4472.
- S2. C. Choi, S. Kwon, T. Cheng, M. Xu, P. Tieu, C. Lee, J. Cai, H. M. Lee, X. Pan, X. Duan, W. A. Goddard and Y. Huang, *Nat. Catal.*, 2020, **3**, 804–812.
- S3. L. Wang, S. Nitopi, A. B. Wong, J. L. Snider, A. C. Nielander, C. G. Morales-Guio, M. Orazov, D. C. Higgins, C. Hahn and T. F. Jaramillo, *Nat. Catal.*, 2019, **2**, 702–708.
- S4. D. Zhong, Z.-J. Zhao, Q. Zhao, D. Cheng, B. Liu, G. Zhang, W. Deng, H. Dong, L. Zhang, J. Li, J. Li and J. Gong, *Angew. Chem. Int. Ed.*, 2021, **60**, 4879–4885.
- S5. T. T. H. Hoang, S. Verma, S. Ma, T. T. Fister, J. Timoshenko, A. I. Frenkel, P. J. A. Kenis and A. A. Gewirth, *J. Am. Chem. Soc.*, 2018, **140**, 5791–5797.
- S6. J.-J. Lv, M. Jouny, W. Luc, W. Zhu, J.-J. Zhu and F. Jiao, *Adv. Mater.*, 2018, **30**, 1803111.
- S7. S. Ma, M. Sadakiyo, R. Luo, M. Heima, M. Yamauchi and P. J. A. Kenis, *J. Power Sources*, 2016, **301**, 219–228.
- S8. Z. Chen, T. Wang, B. Liu, D. Cheng, C. Hu, G. Zhang, W. Zhu, H. Wang, Z.-J. Zhao and J. Gong, *J. Am. Chem. Soc.*, 2020, **142**, 6878–6883.
- S9. T. T. H. Hoang, S. Ma, J. I. Gold, P. J. A. Kenis and A. A. Gewirth, *ACS Catal.*, 2017, **7**, 3313–3321.
- S10. Y. Wang, H. Shen, K. J. T. Livi, D. Raciti, H. Zong, J. Gregg, M. Onadeko, Y. Wan, A. Watson and C. Wang, *Nano Lett.*, 2019, **19**, 8461–8468.
- S11. Z. Li, R. M. Yadav, L. Sun, T. Zhang, J. Zhang, P. M. Ajayan and J. Wu, *Appl. Catal., A*, 2020, **606**, 117829.